Appl. Phys. B 29, 37–42 (1982)

Applied Physics B Photophysics and Laser Chemistry

Four-Wave Mixing in Alkali Halide Crystals and Aqueous Solutions

A. Penzkofer, J. Schmailzl, and H. Glas

Naturwissenschaftliche Fakultät II – Physik, Universität Regensburg, D-8400 Regensburg, Fed. Rep. Germany

Received 12 March 1982/Accepted 3 May 1982

Abstract. Noncollinear phase-matched nonresonant four-photon frequency mixing $\omega_P+\omega_P-\omega_L\rightarrow\omega_S$ in crystals and aqueous solutions of LiCl, CsCl, KF, and KI is studied. The concentration of the aqueous solutions is varied between 0.5 mol/l and saturation. Picosecond laser pulses of a mode-locked Nd-glass laser are applied as pump pulses. The energy conversion of laser light at frequency ω_L to frequency ω_S is measured and the nonlinear susceptibilities $\chi^{(3)}$ are calculated. The dependence of the hyperpolarizabilities on concentration is analysed and gives information on the solute-solvent interaction.

PACS: 42.65, 61.20

Noncollinear phase-matched nonresonant four-photon frequency mixing $\omega_P+\omega_P-\omega_L\rightarrow\omega_S$ in water has been studied recently [1]. Picosecond laser pulses of a mode-locked Nd-glass laser at frequencies $\tilde{\nu}_L=9480\ \mathrm{cm}^{-1}$ (fundamental) and $\tilde{\nu}_P=18{,}960\ \mathrm{cm}^{-1}$ (second harmonic) were used as pump pulses and picosecond light pulses at frequency $\tilde{\nu}_S=28{,}440\ \mathrm{cm}^{-1}$ were generated.

In this paper alkali halide crystals and aqueous alkali halide solutions are used as nonlinear media [2]. LiCl, CsCl, KF, and KI are selected to span a wide range of cations and anions. The concentration of the aqueous solutions is varied between 0.5 mol/l and saturation. The energy conversions are measured and the nonlinear susceptibilities $\chi^{(3)}$ are calculated in the same manner as reported earlier [1]. The hyperpolarizabilities of the alkali halides are determined from the nonlinear susceptibility values. Their dependence on concentration is discussed.

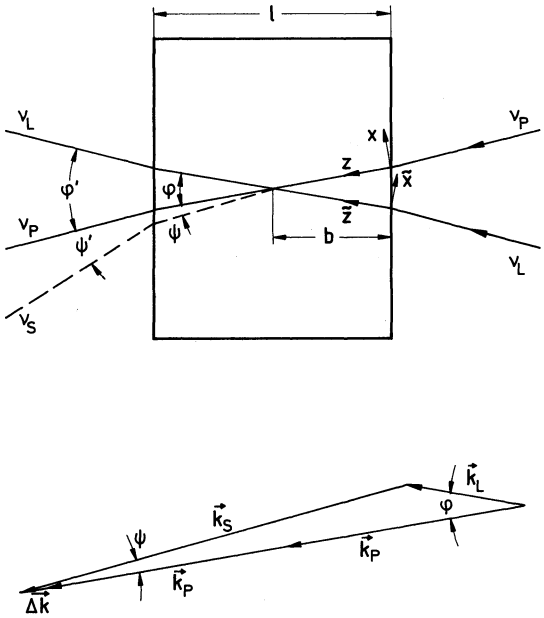

Fig. 1. Geometrical arrangement of laser beams in sample and phase-matching triangle

1. Experiments

The experimental set-up is the same as described previously [1]. The interaction process $\omega_P+\omega_P-\omega_L\rightarrow\omega_S$ is studied. The input picosecond pump pulses are generated by a mode-locked Nd-glass laser. A noncollinear geometry is used to achieve phase-matching as is depicted in Fig. 1. The input beams are focused with cylindrical lenses to obtain long interaction lengths at elevated intensities. The generated picosecond light pulses at frequency ν_S are detected with a photomultiplier tube. The photomultiplier and photodetector signals are registered with a computerized analogue-to digital converter system [3].

0721-7269/82/0029/0037/$01.20

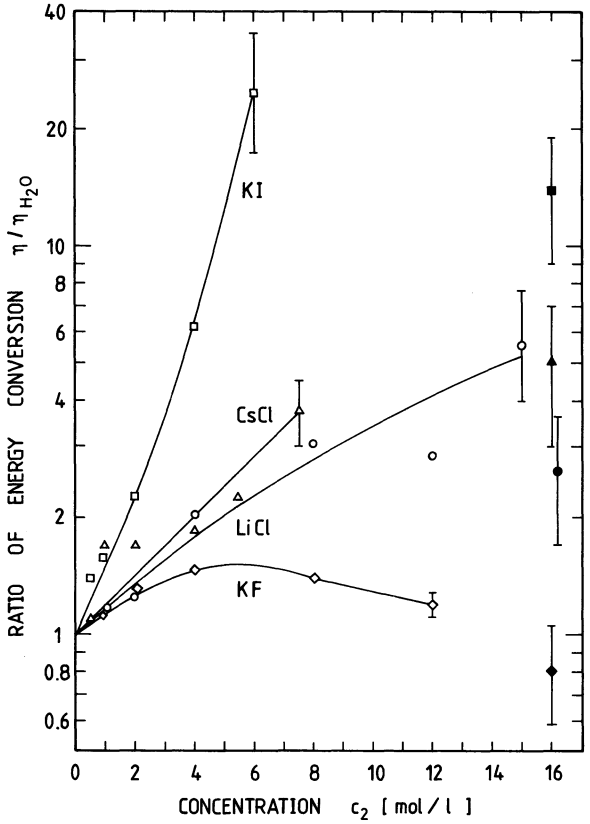

Fig. 2. Dependence of energy conversion on electrolyte concentration. Data are normalized to energy conversion of neat water. Crystal values are included at right hand side (full symbols). $T=25\,^{\circ}C$, sample length $l=2\,cm$

The parameters of the pump pulses are the same as reported earlier [durations $\Delta t_L=6\,ps$ (FWHM), $\Delta t_P=5\,ps$; cross-sections $\Delta x_L=7\,mm$, $\Delta y_L=0.11\,mm$, $\Delta x_P=4.7\,mm$, $\Delta y_P=0.12\,mm$; beam divergence outside cell $\Delta\Theta'_L=4\times10^{-4}\,rad$, $\Delta\Theta'_P=2\times10^{-4}\,rad$]. The peak intensity I_{OP} of the pump pulses at frequency ν_P is in the range between 1×10^9 and $4\times10^9\,W/cm^2$. Both input pump pulses are linear polarized in the vertical direction (y-axis).

The sample length is $l=2\,cm$. The temperature is set to $T=25\,^{\circ}C$. The crystals and the aqueous solutions are enclosed in cells with windows of quartz glass. The hygroscopic crystals are imbedded in nonpolar liquids (LiCl and CsCl in cyclohexane, KF in isopropanol, KI in toluene).

The efficiency of energy conversion $\eta=W_S/W_L$ is measured. Figure 2 shows the results. The energy conversion is normalized to the energy conversion of neat water at the same input peak intensity I_{OP} [$\eta(H_2O)\simeq3\times10^{-4}$ at $I_{OP}\simeq3\times10^9\,W/cm^2$]. The energy conversion of the solids is smaller than the energy conversion of the saturated aqueous solutions (approximately equal in case of CsCl). The energy conversion of KF solutions has a maximum at about 6 mol/l and decreases to the solid state value at higher concentration. In saturated KI solution the energy conversion is increased by a factor of about twenty-five compared to water.

2. Nonlinear Susceptibilities

The four-photon frequency mixing process $\omega_P+\omega_P-\omega_L\rightarrow\omega_S$ is caused by the third-order nonlinear polarization

$$P_{NL}^{(3)}=3\varepsilon_0\chi^{(3)}_{yyyy}(-\omega_S;\omega_P,\omega_P,-\omega_L)E_P^2E_L^*\exp(-i\mathbf{\Delta k r}). \quad (1)$$

In (1) the nonlinear susceptibility $\chi^{(3)}$ is defined according to [4], i.e. $\mathbf{P}_{NL}^{(3)}=4\varepsilon_0\chi^{(3)}\vdots\mathbf{EEE}$ (in [1] we used $\mathbf{P}_{NL}^{(3)}=\chi^{(3)}\vdots\mathbf{EEE}$ [5]).

A relation between the measured energy conversion $\eta(\varphi)$ and the nonlinear susceptibility $\chi^{(3)}_{yyyy}(-\omega_S;\omega_P,\omega_P,-\omega_L)$ [abbreviated $\chi^{(3)}$] was derived in [1]. The energy conversion at an angle φ_0 and a time delay t_D between the input pulses is given by

$$\eta(\varphi_0,t_D)=\frac{4\times3^{1/2}\pi^2\tilde{\nu}_S^2|\chi^{(3)}|^2I_{OP}^2l^2K(\varphi_0,t_D)}{n_Sn_P^2n_Lc^2\varepsilon_0^2\cos(\psi)}. \quad (2)$$

The function $K(\varphi_0,t_D)$ describes the reduction of energy conversion due to phase-mismatch, imperfect temporal and spatial overlap as well as angular spread of the light pulses. One finds (Gaussian profiles are assumed)

$$K(\varphi_0,t_D)=\frac{4\times3^{3/2}\ln(2)}{\pi l^2\Delta x_L\Delta t_L(1+2\Delta y_L^2/\Delta y_P^2)^{1/2}}\cdot\int_{-\infty}^{\infty}f(\varphi-\varphi_0)g(\varphi,t_D)d\varphi. \quad (3)$$

$f(\varphi-\varphi_0)$ describes the effect of the finite divergence of the light beams on the energy conversion. For an angular spread of the input pulses inside the sample of $\Delta\Theta_L$ and $\Delta\Theta_P$ (FWHM), $f(\varphi-\varphi_0)$ is given by

$$f(\varphi-\varphi_0)=\frac{2(\ln2)^{1/2}}{\pi^{1/2}\Delta\Theta_0}\cdot\exp[-4\ln(2)(\varphi-\varphi_0)^2/\Delta\Theta_0^2]. \quad (4)$$

It may be approximated by $f(\varphi-\varphi_0)=1/\Delta\Theta_0$ for $-\Delta\Theta_0/2\leqq\varphi-\varphi_0\leqq\Delta\Theta_0/2$ and 0 otherwise [$\Delta\Theta_0=(\Delta\Theta_L^2+\Delta\Theta_P^2)^{1/2}$].

$g(\varphi,t_D)$ takes into account the phase-mismatch and

integrates over the temporal and spatial pulse shapes

$$g(\varphi, t_D) = \frac{\sin^2(\Delta k_x \Delta x/2)}{(\Delta k_x \Delta x/2)^2} \cdot \int_{-\infty}^{\infty}\int_{-\infty}^{\infty}\left|\int_0^{\tilde{l}} \exp\left\{-\frac{x^2}{x_P^2} - \frac{(t-n_{gP}z/c)^2}{t_P^2} - \alpha_P z - \frac{1}{2}\left[\frac{\tilde{x}^2}{x_L^2} + \frac{(t-t_D-n_{gL}\tilde{z}/c)^2}{t_L^2} + \alpha_L \tilde{z}\right] - \frac{n_{gS}\alpha_S}{2n_S\cos(\psi)}(\tilde{l}-z) - i[\Delta k_z - \Delta k_x \tan(\psi)]z\right\} dz\right|^2 dx'\,dt', \quad (5)$$

where $x_i = \Delta x_i(\ln 2)^{-1/2}/2$, $t_i = \Delta t_i(\ln 2)^{-1/2}/2$ $(i = \mathrm{L}, \mathrm{P})$,

$x = x' - \tan(\psi)z$, $t = t' + n_{gS}^2 z/[n_S c\cos(\psi)]$,

$\tilde{x} = x\cos\varphi - z\sin\varphi + 2b\sin(\varphi/2)$,

$\tilde{z} = z\cos\varphi + x\sin\varphi - 2b\tan(\varphi/2)\sin(\varphi/2)$,

$b = l/2$ (Fig. 1).

$\psi = \arcsin\{n_L\tilde{\nu}_L\sin\varphi/[(n_L\tilde{\nu}_L)^2 + (2n_P\tilde{\nu}_P)^2 - 4n_L n_P\tilde{\nu}_L\tilde{\nu}_P\cos\varphi]^{1/2}\}$, $\tilde{l} = l/\cos(\varphi/2)$,

$\Delta x = \lambda_S/\Delta\Theta_S \simeq \lambda_P/\Delta\Theta_P = 1/(\tilde{\nu}_P n_P \Delta\Theta_P)$.

$\Delta k_x = k_L\sin\varphi - k_S\sin\psi$,

$\Delta k_Z = k_L\cos\varphi + k_S\cos\psi - 2k_P$,

$(k_i = n_i\omega_i/c = 2\pi n_i\nu_i/c = 2\pi n\tilde{\nu}_i)$.

n_i and n_{gi} $(i = \mathrm{S}, \mathrm{P}, \mathrm{L})$ are the phase and group refractive indices, respectively. α_i are the absorption coefficients. t_D describes the temporal delay between the pump pulses at the entrance face of the sample. The

$$\sin^2(\Delta k_x \Delta x/2)/(\Delta k_x \Delta x/2)^2$$

term results from interference of the electrical field strength $\mathbf{E}_S$ within the diffraction limited divergence [6]. At phase-matching φ_0 is

$$\varphi_{opt} = \arccos\{[(2n_P\tilde{\nu}_P)^2 + (n_L\tilde{\nu}_L)^2 - (n_S\tilde{\nu}_S)^2]/(4n_P n_L\tilde{\nu}_P\tilde{\nu}_L)\}.$$

The function K would be equal to one for the idealized case of collinear phase-matched interaction ($\varphi_{opt} = 0$, $\alpha_i = 0$, $\Delta\Theta_0 = 0$, $\mathbf{\Delta k} = 0$, $n_i = n_{gi} = $ constant, $t_D = 0$, $\Delta t_P = \Delta t_L$, $\Delta x_L = \Delta x_P$, $\Delta y_L = \Delta y_P$).

The effective divergence $\Delta\Theta_0$ inside the sample is slightly smaller than the divergence $\Delta\Theta_0'$ outside the sample [1]. [$\Delta\Theta_0 = \Delta\Theta_0'\cos\varphi'/(n_P\cos\varphi)$, $\Delta\Theta_0' = 4.5 \times 10^{-4}$ rad, $\Delta\Theta_0 \simeq 3.3 \times 10^{-4}$ rad.] The half width $\Delta\varphi$ of $g(\varphi)$ decreases with increasing phase matching angle φ_{opt} and effective interaction length l_{eff}. Since l_{eff} reduces with φ_{opt}, the acceptance angle $\Delta\varphi$ is found to be approximately constant. For the investigated substances $\Delta\varphi$ lies between 1.6×10^{-4} and 1.4×10^{-4} rad (solid KI: $\Delta\varphi \simeq 1 \times 10^{-4}$ rad). The small half width $\Delta\varphi$ reduces the conversion efficiency (K is proportional to $\Delta\varphi/\Delta\Theta_0$).

Table 1 summarizes the parameters involved in (2)–(5). φ_{opt} is calculated from the measured external phase-matching angle φ'_{opt}. The refractive indices have been determined in [7]. The absorption coefficients have been measured with a spectral photometer. The calculated $K(\varphi_{opt}, t_{D,opt})$ values for optimum pulse overlap are included in the table. K decreases with increasing φ_{opt} from $K \simeq 0.13$ at $\varphi_{opt} \simeq 10°$ to $K \simeq 0.006$ at $\varphi_{opt} \simeq 25°$.

The $\chi^{(3)}$-values of the aqueous alkali halide solutions versus concentration are depicted in Fig. 3. The $\chi^{(3)}$-data of the alkali halide crystals are inserted. The nonlinear susceptibilities are normalized to the susceptibility of water $\chi^{(3)}(H_2O) = 2 \times 10^{-23}\,m^2/V^2$ $(= 1.5 \times 10^{-15}$ esu).

The nonlinear susceptibilities of LiCl, CsCl, and KI increase with concentration towards the crystal values. The nonlinear susceptibility of saturated KI solution is about a factor of fifteen greater than the value of liquid water. The nonlinear susceptibility of the KI crystal $\chi^{(3)}(\mathrm{KI}) = (4.8 \pm 1.4) \times 10^{-22}\,m^2/V^2$ agrees well with a previously reported value of $\chi^{(3)}(\mathrm{KI}) = 5.8 \times 10^{-22}\,m^2/V^2$ $(= 4.4 \times 10^{-14}$ esu) [8, 9]. The KF solutions show a maximum in the concentration dependence of $\chi^{(3)}$ at about 6 mol/l. At higher concentrations $\chi^{(3)}$ decreases towards the crystal value.

3. Apparent Hyperpolarizabilities

The nonlinear polarization $P_{NL}^{(3)}$ may be expressed in terms of nonlinear susceptibilities $\chi^{(3)}$ or in terms of average hyperpolarizabilities γ [10, 11]

$$\mathbf{P}_{NL}^{(3)} = 4\varepsilon_0\chi^{(3)}\vdots\mathbf{EEE} = \tfrac{1}{6}\mathrm{NL}^4\gamma\vdots\mathbf{EEE}. \quad (6)$$

In our special case of four photon frequency mixing it is

$$\gamma_{yyyy}(-\omega_S;\omega_P,\omega_P,-\omega_L) = \frac{24\varepsilon_0}{\mathrm{NL}^4}\chi^{(3)}_{yyyy}(-\omega_S;\omega_P,\omega_P,-\omega_L). \quad (7)$$

$L^4 = (n_L^2+2)(n_P^2+2)^2(n_S^2+2)/3^4$ is the Lorentz local field correction factor. $N = N_A\varrho/M$ represents the number density of particles. $N_A = 6.022169 \times 10^{23}\,\mathrm{mol}^{-1}$ is the Avogadro number, ϱ the density [g/cm^3] and M the molar mass [g/mol].

Table 1. Data for calculation of $\chi^{(3)}$ [Eqs. (2)–(5)]

c [mol/l]	φ_{opt} [°]	n_S	n_P	n_L	n_{gS}	n_{gP}	n_{gL}	α_S [cm^{-1}]	α_P	α_L	$t_{D,opt}$ [ps]	$K(\varphi_{opt})$
H_2O $M=18.0153$ g/mol												
55.34	10.68	1.34815	1.33468	1.3247	1.39823	1.35783	1.33518	2.3×10^{-3}	3.2×10^{-4}	0.172	2.3	0.113
LiCl $M=42.392$ g/mol												
1	11.07	1.3581	1.3437	1.3332	1.4111	1.3686	1.3455	0.0025	3×10^{-4}	0.171	2.4	0.113
2	11.38	1.3671	1.3519	1.3410	1.4238	1.3781	1.3535	0.003	3×10^{-4}	0.170	2.5	0.106
4	11.97	1.3847	1.3678	1.3562	1.4487	1.3965	1.3690	0.004	3×10^{-4}	0.169	2.8	0.094
8	12.83	1.4179	1.3984	1.3855	1.4938	1.4309	1.3988	0.009	3×10^{-4}	0.165	3.3	0.074
12	13.41	1.4505	1.4289	1.4151	1.5359	1.4646	1.4286	0.014	3×10^{-4}	0.158	3.8	0.060
15	13.66	1.4738	1.4511	1.4368	1.5640	1.4883	1.4503	0.018	3×10^{-4}	0.152	4.2	0.052
Solid	16.90	1.7058	1.6677	1.6468	1.8714	1.7273	1.6604	0.004	0.01	0.07	7.2	0.036
CsCl $M=168.358$ g/mol												
1	11.12	1.3625	1.3479	1.3374	1.4161	1.3730	1.3496	0.009	3×10^{-4}	0.168	2.5	0.112
2	11.53	1.3750	1.3593	1.3483	1.4336	1.3861	1.3607	0.01	3×10^{-4}	0.164	2.8	0.106
4	12.26	1.4002	1.3824	1.3705	1.4682	1.4122	1.3830	0.012	3×10^{-4}	0.156	3.2	0.094
5.5	12.77	1.4186	1.3993	1.3867	1.4939	1.4314	1.3993	0.015	3×10^{-4}	0.150	3.6	0.084
7.5	13.36	1.4449	1.4236	1.4102	1.5295	1.4586	1.4229	0.022	3×10^{-4}	0.143	4.1	0.074
Solid	17.18	1.6842	1.6454	1.6243	1.8539	1.7060	1.6380	0.02	0.01	0.06	6.4	0.035
KF $M=58.1004$ g/mol												
1	10.74	1.3529	1.3393	1.3293	1.4023	1.3630	1.3413	0.012	3×10^{-4}	0.175	2.3	0.113
2	10.79	1.3582	1.3444	1.3342	1.4084	1.3684	1.3463	0.015	3×10^{-4}	0.178	2.3	0.113
4	10.81	1.3645	1.3506	1.3405	1.4150	1.3747	1.3524	0.018	3×10^{-4}	0.181	2.3	0.11
8	10.70	1.3727	1.3591	1.3493	1.4226	1.3827	1.3606	0.014	3×10^{-4}	0.179	2.3	0.11
12	10.65	1.3768	1.3633	1.3538	1.4263	1.3864	1.3645	0.011	3×10^{-4}	0.176	2.3	0.111
Solid	9.62	1.3750	1.3645	1.3585	1.4153	1.3809	1.3625	0	0	0.3	1.7	0.133
KI $M=166.0064$ g/mol												
0.5	11.67	1.3612	1.3453	1.3342	1.4212	1.3723	1.3469	0.012	3×10^{-4}	0.168	2.7	0.101
1	12.59	1.3750	1.3567	1.3445	1.4467	1.3872	1.3578	0.023	3×10^{-4}	0.165	3.1	0.085
2	14.20	1.4008	1.3777	1.3632	1.4962	1.4151	1.3778	0.051	3×10^{-4}	0.161	3.9	0.057
4	16.70	1.4512	1.4191	1.4005	1.5928	1.4695	1.4172	0.184	3×10^{-4}	0.152	5.5	0.024
6	18.89	1.5020	1.4605	1.4377	1.6955	1.5247	1.4566	0.20	3×10^{-4}	0.144	7.3	0.013
Solid	25.42	1.7625	1.6778	1.6358	2.2345	1.8067	1.6624	0.02	0	0.05	16	0.0062

For solutions (binary mixtures) the nonlinear susceptibility is composed of solvent (γ_1) and solute (γ_2) contributions

$$\chi^{(3)}=\frac{N_A L^4}{24\varepsilon_0 1000}(c_1\gamma_1+c_2\gamma_2) \tag{8}$$

$c_1=(1000\varrho-c_2M_2)/M_1$ is the concentration of the solvent; ϱ the density of the solution and c_2 the concentration of the solute.

The hyperpolarizabilities γ_1 and γ_2 may depend on the concentration c_2 (see later). Since γ_1 and γ_2 are not measured separately, we replace γ_1 by γ_0 the hyperpolarizability of the neat solvent and compile concentration dependent contributions of γ_1 in an apparent hyperpolarizability γ_2' of the solute

$$\chi^{(3)}=\frac{N_A L^4}{24\varepsilon_0 1000}(c_1\gamma_0+c_2\gamma_2')$$

$$=\frac{L^4}{L_0^4}\frac{c_1}{c_0}\chi_0^{(3)}+\frac{N_A L^4}{24\varepsilon_0 1000}c_2\gamma_2'. \tag{9}$$

The index 0 stands for neat water. γ_0 is calculated from the nonlinear susceptibility $\chi_0^{(3)}$ with aid of (7) to be $\gamma_0=5\times10^{-62}\,\mathrm{Asm^4/V^3}$.

The normalized apparent hyperpolarizabilities γ_2'/γ_0 of aqueous alkali halide solutions are depicted in Fig. 4. The γ_2/γ_0 values of the crystals are included. The hyperpolarizabilities γ_2' of the solutions are larger than the corresponding crystal values. γ_2' of KI solutions increases with concentration from $\gamma_2'/\gamma_0\simeq28$ at $c_2=0$ mol/l to $\gamma_2'/\gamma_0\simeq80$ at $c_2=6$ mol/l. The hyperpolarizabilities of CsCl and LiCl are approximately independent of concentration. In case of KF γ_2' decreases with concentration from $\gamma_2'/\gamma_0\simeq6$ at 0 mol/l to $\gamma_2'/\gamma_0\simeq1.3$ at 12 mol/l (crystal value $\gamma_2/\gamma_0\simeq1.1$).

The apparent hyperpolarizabilities of the aqueous solutions seem to be mainly determined by the anions, since the CsCl and LiCl values at a fixed concentration differ only slightly while the KF and KI values are strongly different.

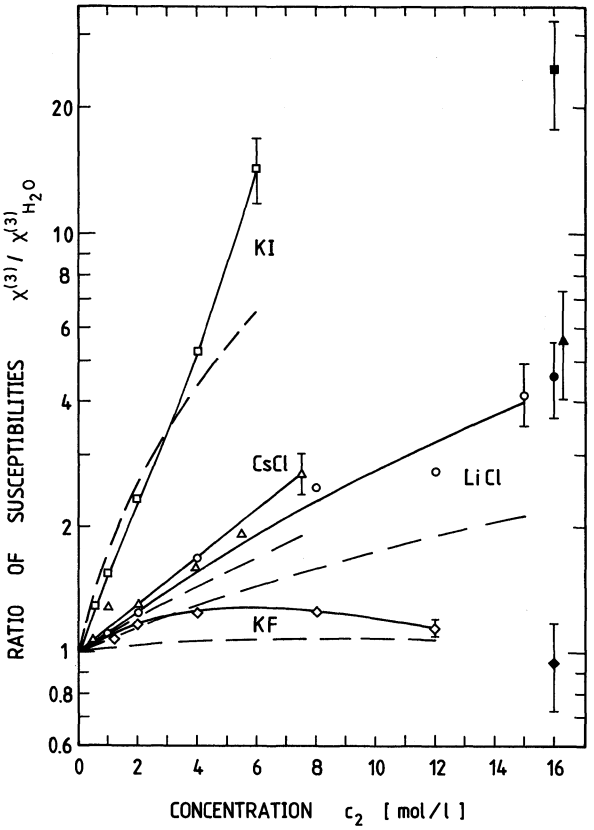

Fig. 3. Dependence of nonlinear susceptibility on electrolyte concentration. Crystal data are included at right hand side (full symbols). The nonlinear susceptibilities are normalized to $\chi^{(3)}(H_2O) \simeq 2 \times 10^{-23}\,m^2/V^2$. Points and solid curves are calculated from energy conversion of Fig. 2. Dashed curves are calculated from generalized Miller's rule (14)

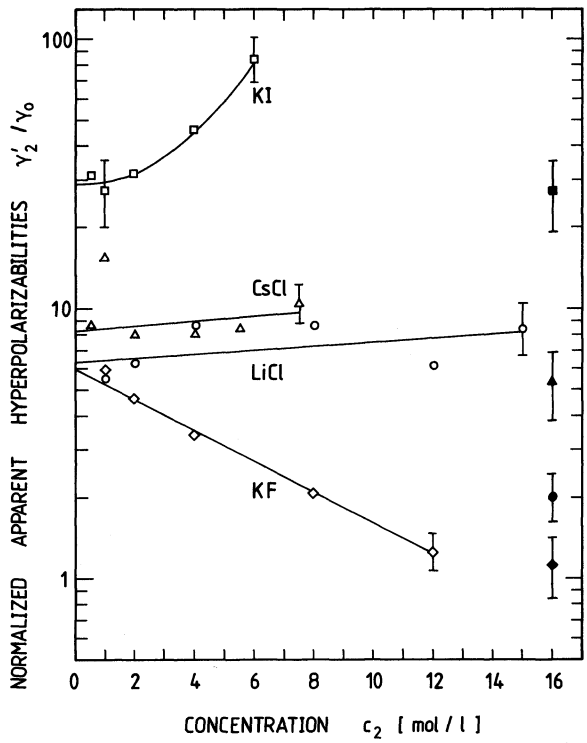

Fig. 4. Normalized hyperpolarizabilities versus concentration of alkali halides. Crystal values at right hand side (full symbols). $\gamma_0 = \gamma(H_2O) \simeq 5 \times 10^{-62} Asm^4/V^3$

4. Intrinsic and Interaction Hyperpolarizabilities

The hyperpolarizability of particles in condensed phase may be split into intrinsic and interaction contributions $\gamma = \gamma^{(g)} + \gamma^{(i)}$. The intrinsic part $\gamma^{(g)}$ is the hyperpolarizability of the gaseous state. The interaction contribution $\gamma^{(i)}$ results from the mutual interaction of neighbouring particles.

In case of solutions the nonlinear susceptibility may be expressed as [7]

$$\chi^{(3)} = \frac{N_A L^4}{24\varepsilon_0 1000}[c_1(\gamma_1^{(g)} + X_1\gamma_{11}^{(i)}) + c_2(\gamma_2^{(g)} + X_2\gamma_{22}^{(i)}) + (c_1 + c_2)X_1X_2\gamma_{12}^{(i)}]. \quad (10)$$

$X_i = c_i/(c_1 + c_2)(i = 1, 2)$ are the mole fractions, $\gamma_1^{(g)}$ and $\gamma_2^{(g)}$ represent the intrinsic hyperpolarizabilities, $\gamma_{11}^{(i)}$ is the solvent-solvent, $\gamma_{22}^{(i)}$ the solute-solute, and $\gamma_{12}^{(i)}$ the solvent-solute interaction hyperpolarizability.

The apparent hyperpolarizability γ'_2 is related to the intrinsic and interaction components by, see (10) and (9),

$$\gamma'_2 = \gamma_{2,n} + X_1(\gamma_{12}^{(i)} - \gamma_{22}^{(i)} - \gamma_{11}^{(i)}). \quad (11)$$

The hyperpolarizability of the neat solvent is $\gamma_0 = \gamma_1^{(g)} + \gamma_{11}^{(i)}$ while the hyperpolarizability of the neat solute is $\gamma_{2,n} = \gamma_2^{(g)} + \gamma_{22}^{(i)}$. At infinite dilution ($c_2 = 0$) the apparent hyperpolarizability reduces to $\gamma'_{2,0} = \gamma_2^{(g)} + \gamma_{12}^{(i)} - \gamma_{11}^{(i)}$. Hyperpolarizability data of gaseous water and alkali halides would be necessary to determine the separate interaction terms $\gamma_{12}^{(i)}$, $\gamma_{22}^{(i)}$, and $\gamma_{11}^{(i)}$.

In Fig. 5 the normalized interaction hyperpolarizabilities $\gamma^{(i)}/\gamma_0 = (\gamma_{12}^{(i)} - \gamma_{22}^{(i)} - \gamma_{11}^{(i)})/\gamma_0$ are plotted versus concentration. $\gamma^{(i)}$ is large indicating the importance of interaction contributions to the hyperpolarizability of aqueous alkali halide solutions.

At infinite dilution ($c_2 = 0$) the interaction hyperpolarizability is largest for KF and weakest for KI. KF is known as a strong structure maker while KI acts as a strong structure breaker [12, 13]. The interaction hyperpolarizability $\gamma^{(i)}$ should be independent of concentration. The observed changes of $\gamma^{(i)}$ with concentration indicate changes of the solvent-solvent, solute-solute and solvent-solute interaction with concentration. These changes of interaction are thought to be due to structural changes of the electrolyte solutions with concentration. It should be noted that, for example, at a concentration of 6 mol/l the average cation-anion distance is only 0.65 nm and the hydration sheaths of the ions [14] overlap. The ionic volumes of

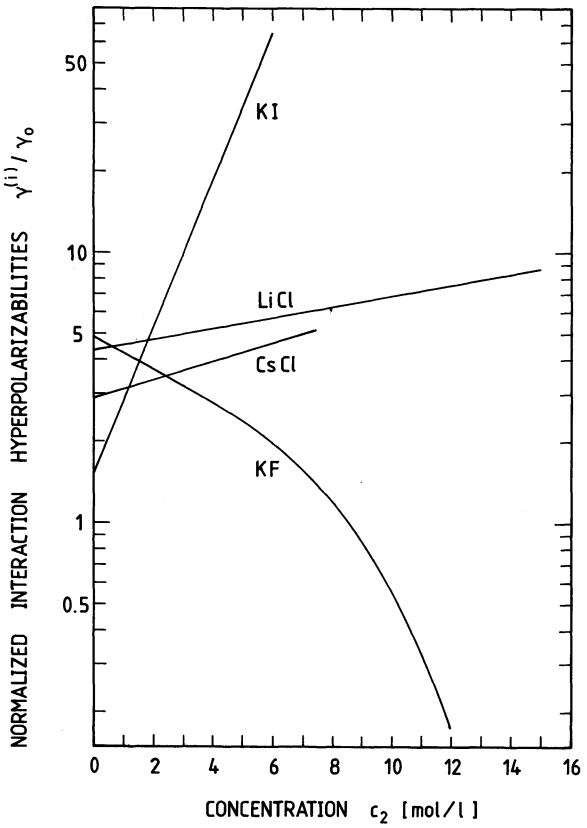

Fig. 5. Normalized interaction hyperpolarizabilities versus concentration of alkali halides. $\gamma^{(i)}=\gamma^{(i)}_{12}-\gamma^{(i)}_{11}-\gamma^{(i)}_{22}=(\gamma'_2-\gamma_{2,n})/X_1$, $\gamma_0=\gamma(H_2O)$. Curves and average solid state values of Fig. 4 are used in calculation of $\gamma^{(i)}$

K^+, Cs^+, F^-, and Cl^- are less than or approximately equal to the voids in water [14]. The particle volume of I^- is larger than the voids and the strongest structural changes with concentration are expected for KI.

5. Anharmonic Oscillator Model

The nonlinear interaction of light fields with particles may be described by an anharmonic oscillator model [11, 15] where the displacement x of electrons is given by $\ddot{x}+\omega_0^2 x-\xi x^3=-f^{1/2}eLE/m$. ($f$ oscillator strength, m electron mass, e electron charge, ω_0 transition frequency, ξ anharmonic coupling constant.) This model leads to the following relation between hyperpolarizability γ and linear polarizability α [$P=P_L+P^{(3)}_{NL}$, $P_L=NL\alpha E=\varepsilon_0\chi^{(1)}E=\varepsilon_0(n^2-1)E$]

$$\gamma(-\omega_S;\omega_P,\omega_P,-\omega_L)=\xi\frac{6m}{f^2e^4}\alpha(\omega_S)\alpha^2(\omega_P)\alpha(\omega_L)$$

$$=\xi\frac{486\varepsilon_0^4 m}{f^2e^4N_A^4}R_SR_P^2R_L. \qquad (12)$$

$R_i=(N_A/3\varepsilon_0)\alpha(\omega_i)$ are the molar refractivities [7, 16].

For neat substances (12) may be rewritten in terms of $\chi^{(3)}$ and $\chi^{(1)}=n^2-1$ (Miller's rule [17])

$$\chi^{(3)}(-\omega_S,\omega_P,\omega_P,-\omega_L)$$

$$=\xi\frac{\varepsilon_0^3 m}{4N^3f^2e^4}(n_S^2-1)(n_P^2-1)^2(n_L^2-1). \qquad (13)$$

The nonlinear susceptibility of solutions changes to the following expression by insertion of (12) into (9)

$$\chi^{(3)}=\frac{L^4}{L_0^4}\frac{c_1}{c_0}\chi_0^{(3)}+c_2\frac{\xi_2}{f_2^2}\frac{81\varepsilon_0^3mL^4}{4000N_A^3e^4}R'_LR'^2_PR'_S. \qquad (14)$$

R'_i are the apparent refractivities [7, 16]. They take into account concentration changes of the linear polarizability. The dashed curves in Fig. 3 are calculated with the aid of (14) (R' values from [7]). The parameter ξ_2/f_2^2 is adjusted to fit the crystal susceptibility values. The deviation of the dashed curves from the measured solid curves indicates that in addition to the changes of $\chi^{(3)}$ determined by the linear polarizability the anharmonic coupling constant ξ_2 is different for crystals and solutions.

Acknowledgements. The authors thank Profs. M. Maier and W. Kaiser for stimulating discussions and T. Ascherl for technical assistance. They are grateful to the "Deutsche Forschungsgemeinschaft" for financial support and to the Rechenzentrum of the University for disposal of computer time.

References

1. A. Penzkofer, J. Kraus, J. Sperka: Opt. Commun. **37**, 437 (1981)
2. M. Becker, R. Fischer, J. Frahm, R. Güther, H. Steudel: Opt. Quant. Electron. **8**, 279 (1976)
3. G. Nibler, A. Penzkofer, W. Blau: Opt. Quant. Electron. **14**, 67 (1982)
4. R.W. Minck. R.W. Terhune, C.C. Wang: Appl. Opt. **5**, 1595 (1966)
5. P.S. Pershan: In *Progress in Optics*, Vol. V, ed. by E. Wolf (North-Holland, Amsterdam 1966) p. 85
6. G.D. Boyd, A. Ashkin, J.M. Dziedzic, D.A. Kleinman: Phys. Rev. **137**, A1305 (1965)
7. A. Penzkofer, H. Glas, J. Schmailzl: Chem. Phys. (in press 1982)
8. P.D. Maker, R.W. Terhune: Phys. Rev. **137**, A801 (1965)
9. C.C. Wang: Phys. Rev. B**2**, 2045 (1970)
10. D.A. Long: *Raman Spectroscopy* (McGraw-Hill, New York 1977)
11. N.L. Boling, A.J. Glass, A. Owyoung: IEEE J. QE-**14**, 601 (1978)
12. *Water a Comprehensive Treatise*, Vol. 3: Aqueous Solutions of Simple Electrolytes, ed. by F. Franks (Plenum Press, New York 1973)
13. *Structure of Water and Aqueous Solutions*, ed. by A.P. Luck (Verlag Chemie, Weinheim 1974)
14. J.O'M. Bockris, A.K.N. Reddy: *Modern Electrochemistry*, Vol. 1 (Plenum Press, New York 1970)
15. F. Zernike, J.E. Mitwinter: *Applied Nonlinear Optics* (Wiley, New York 1973)
16. S.S. Batsanov: *Refractometry and Chemical Structure* (Consultants Bureau, New York 1961)
17. R.C. Miller: Appl. Phys. Lett. **5**, 17 (1964)